

Interfacial Polarons Driven by Charge Transfer In WSe₂/Cuprate Superconductor Systems

Huimin Liu^{1, #}, Tong Yang^{2, #}, Xiongfang Liu^{1, #}, Shengwei Zeng³, Muhammad Fauzi Sahdan⁴, Wenjun Wu¹, Shuo Sun¹, Tengyu Jin¹, Chuanbing Cai¹, Ariando Ariando⁴, Mark B. H. Breese^{4, 5}, Wenjing Zhang⁶, Andrew T. S. Wee^{4, 7}, Chi Sin Tang^{5, *}, Ming Yang^{2, *}, Xinmao Yin^{1, *}

¹Shanghai Key Laboratory of High Temperature Superconductors, Institute for Quantum Science and Technology, Department of Physics, Shanghai University, Shanghai 200444, China

²Department of Applied Physics, The Hong Kong Polytechnic University, Kowloon, Hong Kong, 100872, China

³Institute of Materials Research and Engineering (IMRE), Agency for Science, Technology and Research (A*STAR), 2 Fusionopolis Way, Innovis #08-03, Singapore 138634, Republic of Singapore

⁴Department of Physics, Faculty of Science, National University of Singapore, Singapore 117542

⁵Singapore Synchrotron Light Source (SSLS), National University of Singapore, Singapore 117603

⁶SZU-NUS Collaborative Innovation Center for Optoelectronic Science & Technology, Key Laboratory of Optoelectronic Devices and Systems of Ministry of Education and Guangdong Province, College of Optoelectronic Engineering, Shenzhen University, Shenzhen 518060, China

⁷Centre for Advanced 2D Materials and Graphene Research, National University of Singapore, Singapore 117546

[#]These authors contributed equally to this work.

*To whom correspondence should be addressed: **Chi Sin Tang:** spscst@nus.edu.sg (C.S.T.);

Ming Yang: kevin.m.yang@polyu.edu.hk (M.Y.); **Xinmao Yin:** yinxinmao@shu.edu.cn (X.Y.)

Author Contributions: H.L., T.Y., and X.L. contributed equally to this work. X.Y. conceived the project. H.L., X.L. and C.S.T. performed the PL, Raman and SE experiments and analyzed the data. T.Y., and M.Y. performed the DFT calculations and contributed to the theoretical interpretations. H.L., T.Y., X. L, and C.S.T. wrote the manuscript, with input from all the authors.

Competing Interest Statement: The authors declare no competing financial interest.

Abstract

Understanding the electronic properties of doped copper-oxygen planes remains a significant challenge in condensed matter physics and is crucial to unraveling the mechanisms behind high-temperature superconductivity in cuprates. Recently, the observation of charge transfer and interfacial polarons in superconducting interface has aroused extensive research interest. However, experimental data to investigate charge transfer on the CuO₂ plane and the presence of polarons are still missing. Here we conduct extensive research on the optical and electronic properties of two-dimensional material supported on copper-based superconductors. Unlike monolayer-WSe₂ on other substrates, monolayer-WSe₂ on La_{1.85}Sr_{0.15}CuO₄ (WSe₂/LSCO) produces a special band structure. Using high-resolution spectroscopic ellipsometry and density functional theory calculation methods, the special electronic structure can be attributed to the formation of the interfacial small polaron at the WSe₂/LSCO interface which is driven by charge transfer between the CuO₂ plane of the cuprate superconductor and WSe₂. In addition, the structural phase transition of the LSCO substrate was observed to reduce the electron-hole (e-h) interaction of WSe₂. These findings may spur future investigations on the effect of the interfacial polaron on the superconductivity of cuprates, and highlight the significant influence of interface effects on the electronic structure of WSe₂ films. It provides an effective method to further explore the intrinsic relationship between interfacial polarons and superconductivity.

INTRODUCTION

The pursuit of high-temperature superconductivity has captivated researchers, with copper oxide based unconventional superconductors at the forefront of intense scientific inquiry ¹⁻³. Among these materials, the CuO₂ planes have received considerable attention due to their crucial role in facilitating superconductivity ⁴⁻⁷. Despite this focus, debates persist regarding the fundamental physics governing high-temperature cuprate superconductors, particularly in their normal states ⁸⁻¹⁰. Central to this debate is the intricate interplay of charges on the CuO₂ planes, which has profound implications for the onset and maintenance of superconductivity. While the significance of charge-transfer processes within the CuO₂ planes is widely acknowledged, the underlying mechanisms remain a topic of active investigation ¹¹⁻¹³.

Polarons are quasiparticles that arise due to the presence of intricate interactions between fermionic particles and bosonic fields ¹⁴. Moreover, two different materials are combined into a heterojunction system, interface polaronic coupling may occur. This can regulate the properties of the heterojunction system ¹⁵⁻¹⁷. For example, the dynamical interfacial polarons formed at the FeSe /SrTiO₃ interface are found to play a vital role in enhancing the electron correlation in the overlaying FeSe layer ^{17, 18}. This enhancement phenomenon has also been found at other interfaces, such as FeSe/STO ¹⁹, FeSe/TiO₂ ²⁰, Graphene/h-BN ²¹, etc. The inextricable link between electronic properties of materials and quasiparticle interactions has been further promoted in different material systems ^{18, 22}. Two-dimensional (2D) materials, particularly metal dichalcogenides, have garnered significant attention owing to their fascinating physical properties and potential applications in next-generation electronics, optoelectronics, and topological quantum devices ²³. On the other hand, interfacing 2D materials with cuprate superconductor surfaces may induce various exotic effects. As the superconducting substrates can interact with the overlaying 2D materials through mechanisms such as strain, charge transfer, electric polarization, and magnetism. So 2D materials is an ideal candidate for exploring interfacial phenomena due to its remarkable properties, including a large direct bandgap, easy exfoliation, tunable electronic structure, and susceptibility to charge transfer ²³⁻²⁵. These findings provide compelling evidence for the potential existence of interfacial polarons in two-dimensional/cuprate heterostructure systems. This has direct implications for gaining insight into the underlying mechanisms that cause superconductivity and

other quantum effects to occur, particularly in the functionalization of emerging quantum systems^{26, 27}.

Although experimental evidence of polarons in bulk three-dimensional materials is abundant, they have rarely been observed in two-dimensional crystals²⁸⁻³⁰. Small polaron, due to their stronger electron-phonon coupling, can significantly influence and regulate various properties of two-dimensional materials, including the spin and valley degrees of freedom, superconductivity, and energy gaps^{31, 32}. We also need to understand how manipulation of the lattice and electronic structure through an external medium (such as a substrate) might induce different quantum-mechanical effects at the interface or the two-dimensional layer itself³³.

Here, we report the observation of 2D interfacial small polarons at the heterointerface between monolayer WSe₂ and optimally doped La_{1.85}Sr_{0.15}CuO₄ (LSCO). There are interfacial lattice strain and charge transfer at the heterointerface, and 2D interfacial small polarons have been found (Figure 1a). We further find that the interfacial effect has a significant impact on the band nesting of WSe₂. By utilizing the capabilities of spectroscopic ellipsometry³⁴, we investigate the electronic properties and quasiparticle dynamics. This approach provides crucial insights into the optical response and the identification of interfacial small polarons at the WSe₂/LSCO interface. In particular, detailed analyses indicate that the CuO₂ planes within LSCO are responsible for the interfacial charge transfer from monolayer-WSe₂ into LSCO. These comprehensive experimental and theoretical investigations suggest that strong charge transfer and interfacial strain are likely the key mechanisms driving the formation of interfacial small polarons. This study indicates the important influence of interfacial effects on the electronic structure of WSe₂ thin films. Furthermore, the revelation of interfacial small polarons in this work can stimulate further research to explore the interplay of superconductivity and polaron physics.

RESULTS AND DISCUSSION

Sample Synthesis and Characterization: Large-area monolayer-WSe₂ was synthesized on sapphire (Al₂O₃) substrate by the chemical vapor deposition (CVD) method using WO₃ and Se powders as the reactants ³⁵ and then transferred onto the La_{1.85}Sr_{0.15}CuO₄/LaAlO₃ (LSCO/LAO) system using chemical etchant-assisted wet transfer method (details are provided in the Sample Preparation Section). Meanwhile, temperature-dependent resistivity measurements of the ~87.0 nm LSCO/LAO indicates a superconducting transition (T_C) at 22 K (Figure S1), consistent with previous reports ¹. Figures. 1b and c compare the Raman and photoluminescence (PL) spectra of monolayer-WSe₂ on Al₂O₃ (WSe₂/Al₂O₃) with that of the monolayer-WSe₂ transferred onto the LSCO/LAO film. In the WSe₂/Al₂O₃ system, two main Raman-active modes are observed: (i) The E_{2g}^{1-} -mode (~248 cm⁻¹) associated with in-plane W-Se bond vibrations, and (ii) the A_{1g} -mode (~259 cm⁻¹) originating from out-of-plane Se-Se anti-symmetric vibrations. The positions of these signature modes are consistent with previous reports for monolayer-WSe₂ ³⁶⁻³⁸. Marginal changes in the shape and position shifts of the principal Raman modes can be observed for monolayer-WSe₂ on LSCO/LAO. In particular, the broadening of the E_{2g}^{1-} -mode could be attributed to its widening differences between the constituent E_{2g}^{1+} -mode at a higher wavenumber and the E_{2g}^{1-} -mode at the lower wavenumber ³⁹. Fitting analysis of the original E_{2g}^{1-} -mode (249 cm⁻¹) for the WSe₂/LSCO sample indicates a split into the E_{2g}^{1-} and E_{2g}^{1+} modes, where the former undergoes a redshift to ~242.52 cm⁻¹ while the latter undergoes a blueshift to 250.47 cm⁻¹ (Figure S2 and Supplementary Information Table. 1). The redshift in E_{2g}^{1-} -mode suggests the presence of interfacial tensile strain on monolayer WSe₂ at the WSe₂/LSCO interface ⁴⁰. The out-of-plane A_{1g} -mode does not respond to lattice strain but is sensitive to charge doping. Hence, this redshift in the A_{1g} Raman mode is the characteristic of doped MX₂(M=Mo/W, X=S/Se) and this have been observed in previous studies ⁴⁰⁻⁴². In WSe₂/LSCO, we observe a ~0.68 cm⁻¹ blueshift of the A_{1g} mode to ~259.68 cm⁻¹ (Figure S1a), which indicates the possible effect of charge doping due to its sensitivity to a stronger electron–phonon coupling ⁴³⁻⁴⁶. The observed A_{1g} -mode redshift provides clear evidence of charge transfer at the WSe₂/LSCO interface.

The PL measurement comparison between pristine WSe₂/Al₂O₃ and WSe₂/LSCO exhibits a redshift in the characteristic excitonic transitions from the original ~1.67 eV to ~1.57 eV in WSe₂/LSCO. This may be attributed to a reduction in band gap due to tensile strain ^{47, 48}. Besides the redshift, the PL line shape

changes significantly. Therefore, we perform deconvolution analysis of the PL spectra peaks into their corresponding radiative recombination components (detailed fitting parameters can be found in the Supplementary Information). The neutral exciton X^0 is the ground state of a charge neutral system and trions X^T exciton are the combination of X with one electronic, represented as $e+X^0 \rightarrow X^T$ ⁴⁹. It is clear that the presence of excess charge directly controls the intensity of trion emission⁵⁰. Therefore, charge doping will modulate the relative concentration of trions and neutral excitons in monolayer WSe₂^{51, 52}. To better quantify our findings, the data is fitted with a multipeak model. As shown in Figure S3, the fitting results indicate a significant decrease in the proportion of X^T on WSe₂/LSCO. This indicates a decrease in the electron population of WSe₂. By this, we can infer the onset of charge transfer taking place at the interface. The pronounced changes in the Raman and PL spectra of monolayer WSe₂ upon its transfer onto the LSCO clearly indicate the P-type doping effects of LSCO on WSe₂. It is worth noting that no defect-induced characteristic peaks appear in the Raman spectra of monolayer WSe₂ after transfer, and no defect peaks are observed in the PL spectra (Figure 1a and b). The consistent characterization results indicate that the mechanical transfer process did not introduce significant defects. In addition, the subsequent spectroscopic ellipsometry analysis further confirms the high-quality characteristics of the sample. The spectroscopic ellipsometry of WSe₂ after transfer is highly consistent with the original monolayer WSe₂, and there are no abnormal absorption characteristics within the bandgap caused by defects (such as Urbach tail extension or localized absorption peaks)^{53, 54}. This provides a reliable sample foundation for subsequent research on interface properties.

High-resolution Spectroscopic Ellipsometry Characterization. High-resolution spectroscopic ellipsometry (SE) was conducted to systematically investigate the changes in the optical and excitonic properties that arise due to the interfacial interaction between WSe₂ and LSCO⁵⁵. Figure 2a compares the optical conductivity, σ_1 , of WSe₂/LSCO and the as-prepared WSe₂/Al₂O₃ at 77 K. The shape of the σ_1 spectrum for the as-prepared monolayer-WSe₂ is consistent with results reported in other optical characterization studies^{35, 56-58}. Specifically, it exhibits peaks A, B and C located at \sim 1.67, \sim 2.12 and \sim 2.36 eV, respectively. In the high energy region, a broad band nesting feature labelled D is observed at \sim 2.88 eV. Similar to the PL results, features A and B can be attributed to the excitonic transitions at the K/K' points in the Brillouin zone^{53, 59}. The optical bump feature C may be attributed to the resonant exciton that is formed due to the presence of strong electronic correlations in energy bands above the

optical band gap ⁵³. Meanwhile, the broad feature D is ascribed to the optical transitions in the vicinity of the Γ and M -points of the Brillouin zone where the conduction and valence bands are nested ⁶⁰.

Significant modifications can be observed for the σ_1 spectrum belonging to WSe₂/LSCO despite the persistence of the aforementioned optical features which confirms the quality of the monolayer-WSe₂ after its transfer onto LSCO (Figure 2a). Variations to the σ_1 spectrum suggest that the optical properties and electronic structures of monolayer-WSe₂ have changed due to interfacial interaction taking place at the WSe₂/LSCO interface. Firstly, the intensity of the principle features previously described have undergone an attenuation. Specifically, the band nesting feature D in the photon energy region of ~2.7–3 eV shows a considerable intensity reduction due to changes in the WSe₂ band structure induced by interfacial hybridization and lattice strain which in turn reduces its band nesting structure ⁶⁰. The interfacial effect leads to the reduction in the band nesting structure (around the Γ point) of monolayer-WSe₂. Black curves in the band dispersion indicate a good band nesting area (Figure 1a). Likewise, each optical feature is redshifted and broadened by different extent (Figure 2a). These changes in spectral features are in agreement with the results elucidated from both the Raman and PL and align with previously reported theoretical predictions, which suggest that the reduction in bandgap due to strain originates from the diminished bond angle of Se–W–Se and subsequent changes in orbital overlap ^{47, 48}.

Previous studies indicate that charge doping could cause a redshift in exciton peaks A and B of monolayer-WSe₂ ⁶¹, which in turn implies a possible charge transfer at the WSe₂/LSCO interface. First-principles calculations were then conducted to scrutinize any onset of interfacial charge transfer process. The Fermi level of CuO-terminated LSCO surfaces is ~1 eV below the valence band maximum (VBM) of monolayer-WSe₂ (Figure 2c). This would lead to an interfacial charge transfer from the WSe₂ layer to the CuO-terminated LSCO. Hence, this computational analysis substantiates the experimental results which point to charge transfer at the WSe₂/LSCO interface (see calculation methods in the Supplementary Information for more details). Peak C is a transition from the valence band maximum to the energy band at K-point. Charge transfer and strain effects cause changes to the energy band at this position, resulting in the same red shift and intensity reduction effect as the A and B exciton peaks. Notably, significant changes were observed in a previously unidentified prominent optical shoulder labeled A* at ~1.46 eV exciton A, and its origins will be discussed thereafter.

Temperature-dependent High-resolution Spectroscopic Ellipsometry. Figure 2b displays the optical conductivity, σ_1 , of WSe₂/LSCO at temperatures between 77 and 270 K. Apart from a monotonic reduction in peak intensity, the position and width of the principal excitonic and optical features show a red shifting and broadening trend (Figure S4). These temperature-dependent changes are consistent with previous spectroscopic ellipsometry and reflectance experimental studies of both CVD-grown and exfoliated monolayer TMDs^{53, 62, 63}. The red shifting and broadening behavior of the excitons with increasing temperature can be attributed to processes related to thermal expansion, strengthened electron-phonon interaction, and radiative recombination in monolayer-WSe₂^{64, 65}. In particular, the nonradiative electron-hole recombination process is enhanced as temperature increases and this reduces the probability of radiative transition in monolayer-WSe₂. This contributes significantly to the temperature-dependent variations in the intensity and peak widths that are observed.

Having analyzed the σ_1 spectra, we proceed to discuss the temperature-dependent changes in spectral weights (SW)³⁴. Firstly, emphasis is on the low-energy region (1.30 – 2.18 eV) where the key optical structures are present. To further analyze the temperature-dependence of each optical feature, the photon energy range is further sub-divided into three principal spectral regions where the respective excitons and the additional optical feature A* have been observed. Namely, regions I (1.30–1.48 eV), II (1.48–1.89 eV) and III (1.89–2.18 eV), respectively (See Supplementary Information for details). The SW of the respective optical region can be calculated based on the following expression,

$$SW = (\pi N_{eff} e^2) / (2m_e) = \int_{E_1}^{E_2} \sigma_1(E) dE$$

where N_{eff} denotes the electron density, e denotes the electronic charge, and m_e refers to the electron mass. As shown in Figure 2d, the SW of monolayer-WSe₂/Al₂O₃ in low-energy regions and total region (1.30~3.70 eV) increases linearly with temperature. The changes of the number of the effective carriers are consistent with the spectral weight behavior (Figure S7). This means that the total effective electron density of WSe₂ increases over the entire spectral range, and the number of charges involved in the optical transition increases with temperature^{66, 67}.

However, the SW of monolayer WSe₂/LSCO in total energy region and low-energy regions (I, II, III)

increases first and then decreases around 140 K⁶⁸. It is worth noting that SW of WSe₂/LSCO is similar to the structural transition temperature of LSCO (Figure S5). This indicates that the N_{eff} mutation in the region containing A*, A and B excitons at ~140 K may be related to the structural phase transition of LSCO. Conversely, the spectral weight in the high energy region where the band nesting feature is present (~2.18-3.70 eV) shows a monotonic increase with temperature (See Supplementary Information for details). The temperature-dependent behavior of the spectral weight (or N_{eff}) in the high energy and the low energy region shows opposite behaviors. This could possibly be attributed to the structural phase transition of LSCO has a significant influence on the direct band gap of WSe₂ at the K -point resulting from a change in interfacial lattice strain. The structural transformation has no significant effect on the band nesting structure in the high-energy region⁶⁰.

The Feature A* observed in WSe₂/LSCO heterostructures persists across the entire temperature range (77–270 K). Repeated optical measurements conclusively demonstrate that this feature originates neither from optical artifacts nor defect states in monolayer WSe₂. Its presence throughout the entire temperature range further confirms that structural transformation of LSCO is not the cause of this feature. In addition, monolayer WSe₂ on LSCO is under smaller tensile stress as compared with that when it is on the Al₂O₃ substrate. We can thus eliminate the interfacial lattice strain as the contributing factor to the appearance of feature A* in optical region I. While interlayer excitons appear at a lower energy position compared to excitons from the actual material^{69–71}, the LSCO layer is in metallic state and does not satisfy the conditions for type-II band alignment with WSe₂ which is a necessary condition for the formation of interlayer excitons^{70, 72}. Besides, there is no appearance of excitonic signals in the low-energy region of the PL peak (Figure 1c) which further rules out this possibility. In what follows, we will show that it can be attributed to the interfacial small polarons at the interface between the LSCO and WSe₂ layers.

Bryksin Small-Polaron Model. To further investigate the physical properties of optical feature A* located below exciton A observed in WSe₂/LSCO in the photon energy region between 1.30 and 1.48 eV, curve fitting is performed using the Bryksin small-polaron model (See Supplementary Information for details) which models the electron hopping between in-plane neighboring sites upon activation (Eq. 1 in the Supplementary Information) and its temperature-dependent behavior is analyzed^{73, 74}. The optical responses of the polaron are compatible with the theoretical small-polaron model as seen in the stacked temperature-dependent σ_1 spectra in Figure 3a. As shown in Figure S8, the residual plot results are

consistent with the normal distribution, verifying that the assumptions of the Bryksin model are reasonable. The principal parameters derived from this analysis include the polaron hopping energy, E_a , polaron bandwidth, Γ , and phonon energy, E_{LO} , as displayed in Figures. 3b-d, respectively.

Between 77 and 270 K, the polaron hopping energy between adjacent ion sites (e.g., $W^{2+} \rightarrow W^{2+}$) in WSe₂/LSCO interface exhibits a monotonically increasing trend with increasing temperature from ~ 0.368 eV at 77 K to ~ 0.381 eV at 270 K (Figure 3b). This increase may be attributed to the spreading polaron wave function as temperature increases, which allows for a greater ease of interstitial charge hopping ⁷⁵. Meanwhile, the polaron bandwidth, Γ , also displays a progressive broadening trend with temperature from ~ 0.0687 eV at 77 K to ~ 0.092 eV at 270 K. This is consistent with the behavior of small polarons which corresponds to the phonon broadening trend of the local electronic energy levels and this in turn progressively leads to the broadening of the absorption bands ⁷⁵. Specifically, in WSe₂/LSCO, the small-polaron absorption band broadens with increasing temperature by thermal effects ⁷⁶. The phonon energy, E_{LO} , presents a similar temperature-dependent trend with E_a . As the temperature increases, the lattice vibrations become more intense with rising thermal energy. Nevertheless, the phonon energy remains limited below ~ 15 meV, positioning it relatively close to the acoustic phonon mode of monolayer-WSe₂ and the LSCO substrate ^{68, 77}. This interfacial polaron formation may be attributed to electron-phonon interactions involving transferred holes and the overlapping acoustic phonon modes at the WSe₂/LSCO interface.

Although defect states or interfacial charge transfer may contribute to low-energy optical response, PL characterization (Figure 1c) and spectroscopic ellipsometry experiments (Figure 2b) can effectively rule out their dominant role. There is no new band generated at the peak position. The temperature sensitivity of feature A * is quantitatively consistent with the polaron of the Bryksin model, further supporting its electron-phonon coupling origin. Overall, the compatibility between the optical features observed in the respective σ_1 spectra and the Bryksin small-polaron model strongly suggests that these optical responses genuinely reflect the presence of small polarons at the WSe₂/LSCO heterojunction.

DFT Results of the WSe₂/LSCO Interface. DFT calculations were further performed to shed light on the origins of the small polarons at the WSe₂/LSCO interface. There are two potential origins of the observed polaron and that they might be hosted (i) solely by the *p*-doped WSe₂ on LSCO, or (ii) at the

WSe₂/LSCO interface. In the latter case, excess holes in monolayer-WSe₂ or near the interface could be dressed by the phonons of the LSCO surface according to a penetrating-field mechanism to form interfacial polarons, as observed in other systems such as the SnSe₂/SrTiO₃, FeSe/SrTiO₃ and MoS₂/TiO₂ interfaces¹⁵⁻¹⁷. Based on our DFT calculations as elaborated below, the first proposed origin can be ruled out and this small polaron is more likely the interfacial polaron.

In addition to the charge transfer which leads to the *p*-doping of monolayer-WSe₂, the supported WSe₂ is subjected to structural strain due to lattice mismatch with the LSCO layer. Figure 4a displays the projected band structure of the strain-free WSe₂, where the valence band maximum (VBM) is located at the *K*-point. The Bloch states around VBM at the *K*-point are mainly from the laterally-oriented W- d_{xy} , $d_{x^2-y^2}$ orbitals, while those at the *-point* are mainly from the W- d_{z^2} orbital. Therefore, the application of tensile strains would shift the energy band at the *K*-point downwards and the VBM will be shifted to the *-point* under a tensile strain of at least 4% (Figure 4b). Along with the change in VBM position, the hole effective mass is also greatly enhanced, thereby implying that the excess holes could be self-trapped and localized with greater ease in the WSe₂ layer under tensile strain. By applying a recently developed theoretical model, it can be estimated whether the Fröhlich interaction can stabilize the hole polaron in WSe₂³³. The inequality has been developed as a critical condition for the formation of polarons in 2D materials:

$$\beta = \frac{\epsilon_{ion} \hbar^m d}{m_0 a_0} > 2$$

where ϵ_{ion} , m_h^* , d , m_0 and a_0 denote the ionic contribution to the dielectric constant, the hole effective mass, the effective thickness, the bare electron mass and the Bohr radius, respectively.

As displayed in Figure 4c, the inequality is satisfied for monolayer-WSe₂ when the tensile strain is at least 4%. This is indicative of the existence of the hole polarons in WSe₂ under tensile strains. However, with the estimated polaron radius above ~ 300 Å, the quantum coherence between the electrons and phonons is unlikely to be maintained over such a distance and neither will it be experimentally observable. Attempts were also made to explicitly simulate the hole polaron in both strain-free and 4%-strained WSe₂ supercell at the HSE06 level. However, the excess hole is unable to induce a significant local lattice distortion and be self-trapped in the WSe₂ layer (cyan iso-surface in Figure 4d). Based on these analyses,

WSe₂ alone is unlikely to host a stable hole polaron. Therefore, the experimentally observed polaron could be rooted at the WSe₂/LSCO interface. Wherein, the additional coupling between the holes within WSe₂ or near the interface and the phonons of the LSCO substrate may play a vital role in further stabilizing/localizing the hole polarons.

The SE spectra of monolayer WSe₂/LSCO show a peak A* at 1.5eV which can be well interpreted by interfacial small polarons developed at the interface between WSe₂ and LSCO. Recent studies in FeSe/STO, LaAlO₃/SrTiO₃ have found that interfacial polarons enhance the superconductivity at the interface^{17, 18}. The appearance of polarons at this WSe₂/LSCO heterojunction interface encourages us to compare this interface with similar interfacial superconducting systems. And solid evidence has been recently discovered that interfacial polarons play critical roles in the interfacial conductivity and even enhanced interfacial superconductivity.

Conventional theory holds that polaron formation originates from long-range electron-phonon interactions, which are perceived to facilitate superconducting pairing. However, the precise role of small polarons in the pairing mechanism remains a scientific question to be addressed. Recent experimental and theoretical studies⁷⁸⁻⁸³ have revived interests in the phonon contribution to the pairing mechanism in cuprate superconductors, particularly in the context of strongly correlated electron systems. A theoretical study has suggested that small polarons may promote localized electron pair formation through local electron-phonon coupling⁸⁴, thereby offering an alternative pathway for superconducting pairing.

This work reports the direct observation of interfacial polarons coupled to CuO₂ planes, providing experimental insights into phonon-mediated pairing mechanisms in strongly correlated systems. Notably, the interface-engineered small polarons may modulate local electron-phonon interactions, potentially influencing either the pairing strength or coherence. Understanding the interplay between superconductivity and polaron physics remains highly challenging, and we anticipate that revealing interfacial small polarons in this work may encourage further investigations in this direction.

CONCLUSIONS

In conclusion, we prepared a large monolayer of WSe₂ and transferred it onto a copper-oxide high-temperature superconductor to investigate the properties of the WSe₂/LSCO interface. Our observation

indicates that the WSe₂ on LSCO substrates exhibit a distinctive interface effect compared to on Al₂O₃ substrates. Through a comprehensive investigation that comprises temperature-dependent spectroscopy ellipsometry, Raman spectra, photoluminescence spectra, and DFT calculations, we determined that charge transfer between the CuO₂ plane of LSCO and monolayer-WSe₂ drives the formation of 2D interfacial small polarons. Our work emphasizes the critical role of charge transfer, strain, and interfacial electron-phonon coupling in mediating the formation of these polarons within the WSe₂/LSCO heterostructure. This study is pivotal in advancing our understanding the electronic structures of the CuO₂ plane and for exploring the mechanisms underlying high-temperature superconductivity. It provides important insights into the fundamental physical principles of superconductivity and complex interfacial phenomena. The discovery of interfacial small polarons could stimulate further research to explore the interaction of superconductivity and polaron physics. This study is pivotal in advancing our understanding of the electronic structures of the CuO₂ plane and in exploring the mechanisms underlying high-temperature superconductivity.

Materials and Methods

LSCO: High-quality thin-film La_{1.85}Sr_{0.15}CuO₄ samples were grown on atomically smooth [001]-oriented LaAlO₃ single-crystal substrates, using pulsed laser deposition. The pure cation oxides powders of La₂O₃ (99.999%), Sr₂O₃ (99.997%), and CuO (99.9999%) are used for the preparation of the ceramic target. According to the chemical formula, the materials were weighed and mixed according to the appropriate chemical stoichiometry. Note that the 87.0nm-LSCO/LAO sample is superconducting with T_c~22 K. (Figure S1). This is in good agreement with a previous substrate and thickness-dependent study on the T_c of optimal-doped LSCO films brought about by the effects of epitaxial strain ⁸⁵.

WSe₂: Atomic layers of WSe₂ were synthesized on a sapphire (Al₂O₃) substrate employing the chemical vapor deposition (CVD) technique, utilizing WO₃ and Se powders as reactants. The process involved an annealing step at 200°C to promote intimate contact between the film and substrate while removing any residual impurities. Raman and photoluminescence (PL) spectra WSe₂ monolayers are provided in Supplementary Information Figs.S2 and S3. Comparative analysis with recent reports on monolayer WSe₂ and monolayer WSe₂ on sapphire reveals striking spectral similarities, affirming the high quality of the samples as monolayers.

Chemical etchant-assisted wet transfer methods: The transfer of monolayer-WSe₂ onto the LSCO layer is conducted using polymethyl methacrylate (PMMA). In which case, the PMMA film is spun onto the surface of a WSe₂/Al₂O₃ stack to serve as a mechanical support layer and is left overnight to ensure strong adhesion between the PMMA and the 2D film. Subsequently, the entire stack is immersed in hot deionized (DI) water at an angle of approximately 45° to the water surface. After a few seconds, water begins to penetrate the film/substrate interface due to capillary forces, leading to the delamination of the PMMA/2D film from the substrate⁸⁶. The delaminated film then floats to the surface and is transferred onto an 87.0 nm LSCO/LAO substrate. Following this, the PMMA/WSe₂/LSCO is cleaned using DI water baths and transferred onto the target substrate, after which an acetone bath is employed to dissolve the PMMA support layer.

Data Availability Statement: The data that support the findings of this study are available from the corresponding author upon reasonable request.

Supporting Information: Detailed methodology and analysis of the spectroscopic ellipsometry data, Bryksin small-polaron model and transport measurement data, and additional DFT calculations. Supporting Information is available from the ACS Nano website at DOI: 10.1021/acsnano.5c05277

Acknowledgements

This work was supported by National Key R&D Program of China (Grant No. 2022YFE03150200), the National Natural Science Foundation of China (Grant Nos.52172271, 12374378, 52307026), Shanghai Science and Technology Innovation Program (Grant No. 22511100200, 23511101600). M. Y. acknowledges the funding support from Hong Kong Research Grants Council (project no.: P0046939 and P0045061) and The Hong Kong Polytechnic University (project no.: P0050570, P0048122 and P0047956). C.S.T acknowledges the support from the NUS Emerging Scientist Fellowship. The authors acknowledge the computing resource from the National Supercomputing Centre, Singapore (<https://www.nscc.sg>). This research is supported by the Ministry of Education, Singapore, under MOE-T2EP50124-0003.

References

- (1) Varma, C. M. Colloquium: Linear in temperature resistivity and associated mysteries including high temperature superconductivity. *Rev. Mod. Phys.* **2020**, *92* (3), 031001.
- (2) Lee, P. A.; Nagaosa, N.; Wen, X.-G. J. R. o. m. p. Doping a Mott insulator: Physics of high-temperature superconductivity. *Rev. Mod. Phys.* **2006**, *78* (1), 17.
- (3) Scalapino, D. J. A common thread: The pairing interaction for unconventional superconductors. *Rev. Mod. Phys.* **2012**, *84* (4), 1383-1417.
- (4) Kunisada, S.; Isono, S.; Kohama, Y.; Sakai, S.; Bareille, C.; Sakuragi, S.; Noguchi, R.; Kurokawa, K.; Kuroda, K.; Ishida, Y.; et al. Observation of small Fermi pockets protected by clean CuO₂ sheets of a high T_c superconductor. *Science* **2020**, *369* (6505), 833-838.
- (5) Jiang, K.; Wu, X.; Hu, J.; Wang, Z. J. P. R. L. Nodeless high-T_c superconductivity in the highly overdoped CuO₂ monolayer. *Phys. Rev. Lett.* **2018**, *121* (22), 227002.
- (6) Li, W. M.; Zhao, J. F.; Cao, L. P.; Hu, Z.; Huang, Q. Z.; Wang, X. C.; Liu, Y.; Zhao, G. Q.; Zhang, J.; Liu, Q. Q.; et al. Superconductivity in a unique type of copper oxide. *Proceedings of the National Academy of Sciences* **2019**, *116* (25), 12156-12160.
- (7) Zhang, L.; Zeng, S.; Yin, X.; Asmara, T. C.; Yang, P.; Han, K.; Cao, Y.; Zhou, W.; Wan, D.; Tang, C. S.; et al. The Mechanism of Electrolyte Gating on High-T_c Cuprates: The Role of Oxygen Migration and Electrostatics. *ACS Nano* **2017**, *11* (10), 9950-9956.
- (8) Rybicki, D.; Jurkutat, M.; Reichardt, S.; Kapusta, C.; Haase, J. Perspective on the phase diagram of cuprate high-temperature superconductors. *Nat. Commun.* **2016**, *7* (1), 11413.
- (9) Sarkar, T.; Mandal, P. R.; Poniatowski, N. R.; Chan, M. K.; Greene, R. L. Correlation between scale-invariant normal-state resistivity and superconductivity in an electron-doped cuprate. *Sci. Adv.* **2019**, *5* (5), eaav6753.
- (10) Huang, E. W.; Mendl, C. B.; Liu, S.; Johnston, S.; Jiang, H. C.; Moritz, B.; Devreux, T. P. Numerical evidence of fluctuating stripes in the normal state of high-T_c cuprate superconductors. *Science* **2017**, *358* (6367), 1161-1164..
- (11) O'Mahony, S. M.; Ren, W.; Chen, W.; Chong, Y. X.; Liu, X.; Eisaki, H.; Uchida, S.; Hamidian, M. H.; Davis, J. C. S. On the electron pairing mechanism of copper-oxide high temperature superconductivity. *Proceedings of the National Academy of Sciences* **2022**, *119* (37), e2207449119.
- (12) Lau, B.; Berciu, M.; Sawatzky, G. A. High-Spin Polaron in Lightly Doped CuO₂ Planes. *Phys. Rev. Lett.* **2011**, *106* (3), 036401.
- (13) Freelon, B.; Augustsson, A.; Guo, J. H.; Medaglia, P. G.; Tebano, A.; Balestrino, G. Electron Correlation and Charge Transfer in [(Ba_{0.9}Nd_{0.1})CuO_{2+δ}]₂/[CaCuO₂]₂ Superconducting Superlattices. *Phys. Rev. Lett.* **2006**, *96* (1), 017003.
- (14) Franchini, C.; Reticcioli, M.; Setvin, M.; Diebold, U. Polarons in materials. *Nat. Rev. Mater.* **2021**, *6* (7), 560-586.
- (15) Xiang, M.; Ma, X.; Gao, C.; Guo, Z.; Huang, C.; Xing, Y.; Tan, S.; Zhao, J.; Wang, B.; Shao, X. Revealing the Polaron State at the MoS₂/TiO₂ Interface. *The Journal of Physical Chemistry Letters* **2023**, *14* (14), 3360-3367.
- (16) Mao, Y.; Ma, X.; Wu, D.; Lin, C.; Shan, H.; Wu, X.; Zhao, J.; Zhao, A.; Wang, B. Interfacial Polarons in van der Waals Heterojunction of Monolayer SnSe₂ on SrTiO₃ (001). *Nano Letter* **2020**, *20* (11), 8067-

8073.

(17) Zhang, S.; Wei, T.; Guan, J.; Zhu, Q.; Qin, W.; Wang, W.; Zhang, J.; Plummer, E.; Zhu, X.; Zhang, Z.; et al. Enhanced Superconducting State in FeSe / SrTiO₃ by a Dynamic Interfacial Polaron Mechanism. *Phys. Rev. Lett.* **2019**, *122*.

(18) Song, Q.; Yu, T. L.; Lou, X.; Xie, B. P.; Xu, H. C.; Wen, C. H. P.; Yao, Q.; Zhang, S. Y.; Zhu, X. T.; Guo, J. D.; et al. Evidence of cooperative effect on the enhanced superconducting transition temperature at the FeSe/SrTiO₃ interface. *Nat. Commun.* **2019**, *10* (1), 758.

(19) Zhou, G.; Zhang, D.; Liu, C.; Tang, C.; Wang, X.; Li, Z.; Song, C.; Ji, S.; He, K.; Wang, L.; et al. Interface induced high temperature superconductivity in single unit-cell FeSe on SrTiO₃(110). *Appl. Phys. Lett.* **2016**, *108* (20).

(20) Ding, H.; Lv, Y.-F.; Zhao, K.; Wang, W.-L.; Wang, L.; Song, C.-L.; Chen, X.; Ma, X.-C.; Xue, Q.-K. High-Temperature Superconductivity in Single-Unit-Cell FeSe Films on Anatase TiO₂(001). *Phys. Rev. Lett.* **2016**, *117* (6), 067001.

(21) Chen, C.; Avila, J.; Wang, S.; Wang, Y.; Mucha-Kruczyński, M.; Shen, C.; Yang, R.; Nosarzewski, B.; Devereaux, T. P.; Zhang, G.; et al. Emergence of Interfacial Polarons from Electron–Phonon Coupling in Graphene/h-BN van der Waals Heterostructures. *Nano Lett.* **2018**, *18* (2), 1082-1087.

(22) Lee, J. J.; Schmitt, F. T.; Moore, R. G.; Johnston, S.; Cui, Y. T.; Li, W.; Yi, M.; Liu, Z. K.; Hashimoto, M.; Zhang, Y.; et al. Interfacial mode coupling as the origin of the enhancement of T_c in FeSe films on SrTiO₃. *Nature* **2014**, *515* (7526), 245-248.

(23) Cheng, Q.; Pang, J.; Sun, D.; Wang, J.; Zhang, S.; Liu, F.; Chen, Y.; Yang, R.; Liang, N.; Lu, X.; et al. WSe₂ 2D p-type semiconductor-based electronic devices for information technology: Design, preparation, and applications. *InfoMat* **2020**, *2* (4), 656-697.

(24) Hsu, W.-T.; Lu, L.-S.; Wang, D.; Huang, J.-K.; Li, M.-Y.; Chang, T.-R.; Chou, Y.-C.; Juang, Z.-Y.; Jeng, H.-T.; Li, L.-J.; et al. Evidence of indirect gap in monolayer WSe₂. *Nat. Commun.* **2017**, *8* (1), 929.

(25) Chen, J.-W.; Lo, S.-T.; Ho, S.-C.; Wong, S.-S.; Vu, T.-H.-Y.; Zhang, X.-Q.; Liu, Y.-D.; Chiou, Y.-Y.; Chen, Y.-X.; Yang, J.-C.; et al. A gate-free monolayer WSe₂ pn diode. *Nat. Commun.* **2018**, *9* (1), 3143.

(26) Sekiya, N.; Kobayashi, S. Compact, Low Loss, and High Power Handling HTS Dual-Mode Double-Strip Resonator Filter With New Feeding Structure. *IEEE Trans. Appl. Supercond.* **2019**, *29* (5), 1-4.

(27) Sekiya, N. Design of Compact and High-Power HTS Double-Strip Dual-Mode Patch Resonator Filter for Transmit Filter Applications. *IEEE Trans. Appl. Supercond.* **2017**, *27* (4), 1-4.

(28) Riley, J. M.; Caruso, F.; Verdi, C.; Duffy, L. B.; Watson, M. D.; Bawden, L.; Volckaert, K.; van der Laan, G.; Hesjedal, T.; Hoesch, M.; et al. Crossover from lattice to plasmonic polarons of a spin-polarised electron gas in ferromagnetic EuO. *Nat. Commun.* **2018**, *9* (1), 2305.

(29) Wang, Z.; McKeown Walker, S.; Tamai, A.; Wang, Y.; Ristic, Z.; Bruno, F. Y.; de la Torre, A.; Riccò, S.; Plumb, N. C.; Shi, M.; et al. Tailoring the nature and strength of electron–phonon interactions in the SrTiO₃(001) 2D electron liquid. *Nat. Mater.* **2016**, *15* (8), 835-839.

(30) Chen, C.; Avila, J.; Frantzeskakis, E.; Levy, A.; Asensio, M. C. Observation of a two-dimensional liquid of Fröhlich polarons at the bare SrTiO₃ surface. *Nat. Commun.* **2015**, *6* (1), 8585.

(31) Arsenault, E. A.; Li, Y.; Yang, B.; Wang, X.; Park, H.; Mosconi, E.; Ronca, E.; Taniguchi, T.; Watanabe, K.; Gamelin, D.; et al. Two-Dimensional Moiré Polaronic Electron Crystals. *Phys. Rev. Lett.* **2024**, *132* (12), 126501.

(32) Kang, M.; Jung, S. W.; Shin, W. J.; Sohn, Y.; Ryu, S. H.; Kim, T. K.; Hoesch, M.; Kim, K. S. Holstein polaron in a valley-degenerate two-dimensional semiconductor. *Nat. Mater.* **2018**, *17* (8), 676-680.

(33) Sio, W. H.; Giustino, F. Polarons in two-dimensional atomic crystals. *Nat. Phys.* **2023**, *19* (5), 629-

(34) Yin, X.; Majidi, M. A.; Chi, X.; Ren, P.; You, L.; Palina, N.; Yu, X.; Diao, C.; Schmidt, D.; Wang, B.; et al. Unraveling how electronic and spin structures control macroscopic properties of manganite ultra-thin films. *NPG Asia Mater.* **2015**, *7* (7), e196-e196.

(35) Huang, J. K.; Pu, J.; Hsu, C. L.; Chiu, M. H.; Juang, Z. Y.; Chang, Y. H.; Chang, W. H.; Iwasa, Y.; Takenobu, T.; Li, L. J. Large-area synthesis of highly crystalline WSe₂ monolayers and device applications. *ACS Nano* **2014**, *8* (1), 923-930.

(36) Wang, D.; Zhang, Z.; Huang, B.; Zhang, H.; Huang, Z.; Liu, M.; Duan, X. Few-Layer WS₂-WSe₂ Lateral Heterostructures: Influence of the Gas Precursor Selenium/Tungsten Ratio on the Number of Layers. *ACS Nano* **2022**, *16* (1), 1198-1207.

(37) Zeng, H.; Liu, G.-B.; Dai, J.; Yan, Y.; Zhu, B.; He, R.; Xie, L.; Xu, S.; Chen, X.; Yao, W.; et al. Optical signature of symmetry variations and spin-valley coupling in atomically thin tungsten dichalcogenides. *Sci. Rep.* **2013**, *3*, 1608.

(38) Jin, C.; Kim, J.; Suh, J.; Shi, Z.; Chen, B.; Fan, X.; Kam, M.; Watanabe, K.; Taniguchi, T.; Tongay, S.; et al. Interlayer electron-phonon coupling in WSe₂/hBN heterostructures. *Nat. Phys.* **2017**, *13* (2), 127-131.

(39) Desai, S. B.; Seol, G.; Kang, J. S.; Fang, H.; Battaglia, C.; Kapadia, R.; Ager, J. W.; Guo, J.; Javey, A. Strain-induced indirect to direct bandgap transition in multilayer WSe₂. *Nano Lett.* **2014**, *14* (8), 4592-4597.

(40) Iqbal, M. W.; Shahzad, K.; Akbar, R.; Hussain, G. A review on Raman finger prints of doping and strain effect in TMDCs. *Microelectron. Eng.* **2020**, *219*, 111152.

(41) Cai, L.; McClellan, C. J.; Koh, A. L.; Li, H.; Yalon, E.; Pop, E.; Zheng, X. Rapid Flame Synthesis of Atomically Thin MoO₃ down to Monolayer Thickness for Effective Hole Doping of WSe₂. *Nano Lett.* **2017**, *17* (6), 3854-3861.

(42) Rai, A.; Valsaraj, A.; Movva, H. C. P.; Roy, A.; Ghosh, R.; Sonde, S.; Kang, S.; Chang, J.; Trivedi, T.; Dey, R.; et al. Air Stable Doping and Intrinsic Mobility Enhancement in Monolayer Molybdenum Disulfide by Amorphous Titanium Suboxide Encapsulation. *Nano Lett.* **2015**, *15* (7), 4329-4336.

(43) Corro, E. d.; Terrones, H.; Elias, A.; Fantini, C.; Feng, S.; Nguyen, M. A.; Mallouk, T. E.; Terrones, M.; Pimenta, M. A. Excited Excitonic States in 1L, 2L, 3L, and Bulk WSe₂ Observed by Resonant Raman Spectroscopy. *ACS Nano* **2014**, *8* (9), 9629-9635.

(44) Li, Z.; Wang, Y.; Jiang, J.; Liang, Y.; Zhong, B.; Zhang, H.; Yu, K.; Kan, G.; Zou, M. Temperature-dependent Raman spectroscopy studies of 1-5-layer WSe₂. *Nano Res.* **2020**, *13* (2), 591-595.

(45) Chakraborty, B.; Bera, A.; Muthu, D. V. S.; Bhowmick, S.; Waghmare, U. V.; Sood, A. K. Symmetry-dependent phonon renormalization in monolayer MoS₂ transistor. *Physical Review B* **2012**, *85* (16), 161403.

(46) Tongay, S.; Zhou, J.; Ataca, C.; Lo, K.; Matthews, T. S.; Li, J.; Grossman, J. C.; Wu, J. Thermally Driven Crossover from Indirect toward Direct Bandgap in 2D Semiconductors: MoSe₂ versus MoS₂. *Nano Lett.* **2012**, *12* (11), 5576-5580.

(47) Tang, N.; Du, C.; Wang, Q.; Xu, H. Strain engineering in bilayer WSe₂ over a large strain range. *Microelectron. Eng.* **2020**, *223*, 111202.

(48) Peng, Z.; Chen, X.; Fan, Y.; Srolovitz, D. J.; Lei, D. Strain engineering of 2D semiconductors and graphene: from strain fields to band-structure tuning and photonic applications. *Light Sci. Appl.* **2020**, *9* (1), 190.

(49) Perea-Causin, R.; Brem, S.; Buchner, F.; Lu, Y.; Watanabe, K.; Taniguchi, T.; Lupton, J. M.; Lin,

K.-Q.; Malic, E. Electrically tunable layer-hybridized trions in doped WSe₂ bilayers. *Nat. Commun.* **2024**, *15* (1), 6713.

(50) Gao, S.; Liang, Y.; Spataru, C. D.; Yang, L. Dynamical Excitonic Effects in Doped Two-Dimensional Semiconductors. *Nano Lett.* **2016**, *16* (9), 5568-5573.

(51) Li, Z.; Wang, T.; Lu, Z.; Jin, C.; Chen, Y.; Meng, Y.; Lian, Z.; Taniguchi, T.; Watanabe, K.; Zhang, S.; et al. Revealing the biexciton and trion-exciton complexes in BN encapsulated WSe₂. *Nat. Commun.* **2018**, *9* (1), 3719.

(52) Wang, Z.; Liu, Y.; Chen, D.; Wang, Z.; Asbahi, M.; Rezaei, S. D.; Deng, J.; Teng, J.; Wee, A. T. S.; Zhang, W.; et al. Nanocavity-induced trion emission from atomically thin WSe₂. *Sci. Rep.* **2022**, *12* (1), 15861.

(53) Tang, C. S.; Yin, X.; Yang, M.; Wu, D.; Birowosuto, M. D.; Wu, J.; Li, C.; Hettiarachchi, C.; Chin, X. Y.; Chang, Y.-H.; et al. Three-Dimensional Resonant Exciton in Monolayer Tungsten Diselenide Actuated by Spin-Orbit Coupling. *ACS Nano* **2019**, *13* (12), 14529-14539.

(54) Eichfeld, S. M.; Eichfeld, C. M.; Lin, Y.-C.; Hossain, L.; Robinson, J. A. Rapid, non-destructive evaluation of ultrathin WSe₂ using spectroscopic ellipsometry. *APL Mater.* **2014**, *2* (9), 092508.

(55) D’Innocenzo, V.; Grancini, G.; Alcocer, M. J. P.; Kandada, A. R. S.; Stranks, S. D.; Lee, M. M.; Lanzani, G.; Snaith, H. J.; Petrozza, A. Excitons versus free charges in organo-lead tri-halide perovskites. *Nat. Commun.* **2014**, *5* (1), 3586.

(56) Eichfeld, S. M.; Eichfeld, C. M.; Lin, Y.-C.; Hossain, L.; Robinson, J. A. Rapid, non-destructive evaluation of ultrathin WSe₂ using spectroscopic ellipsometry. *APL Materials* **2014**, *2* (9).

(57) Zhao, W.; Ghorannevis, Z.; Chu, L.; Toh, M.; Kloc, C.; Tan, P.-H.; Eda, G. Evolution of Electronic Structure in Atomically Thin Sheets of WS₂ and WSe₂. *ACS Nano* **2013**, *7* (1), 791-797.

(58) You, Y.; Zhang, X.-X.; Berkelbach, T. C.; Hybertsen, M. S.; Reichman, D. R.; Heinz, T. F. Observation of biexcitons in monolayer WSe₂. *Nat. Phys.* **2015**, *11* (6), 477-481.

(59) Steinleitner, P.; Merkl, P.; Nagler, P.; Mornhinweg, J.; Schüller, C.; Korn, T.; Chernikov, A.; Huber, R. Direct Observation of Ultrafast Exciton Formation in a Monolayer of WSe₂. *Nano Lett.* **2017**, *17* (3), 1455-1460.

(60) Mennel, L.; Smejkal, V.; Linhart, L.; Burgdörfer, J.; Libisch, F.; Mueller, T. Band Nesting in Two-Dimensional Crystals: An Exceptionally Sensitive Probe of Strain. *Nano Lett.* **2020**, *20* (6), 4242-4248.

(61) Pan, Y.; Rahaman, M.; He, L.; Milekhin, I.; Manoharan, G.; Aslam, M. A.; Blaudeck, T.; Willert, A.; Matković, A.; Madeira, T. I.; et al. Exciton tuning in monolayer WSe₂ via substrate induced electron doping. *Nanoscale Adv.* **2022**, *4* (23), 5102-5108.

(62) Peng, X.; Wei, Q.; Copple, A. Strain-engineered direct-indirect band gap transition and its mechanism in two-dimensional phosphorene. *Physical Review B* **2014**, *90* (8), 085402.

(63) Liu, H.-L.; Shen, C.-C.; Su, S.-H.; Hsu, C.-L.; Li, M.-Y.; Li, L.-J. Optical properties of monolayer transition metal dichalcogenides probed by spectroscopic ellipsometry. *Appl. Phys. Lett.* **2014**, *105* (20).

(64) Cadiz, F.; Courtade, E.; Robert, C.; Wang, G.; Shen, Y.; Cai, H.; Taniguchi, T.; Watanabe, K.; Carrere, H.; Lagarde, D.; et al. Excitonic Linewidth Approaching the Homogeneous Limit in MoS₂-Based van der Waals Heterostructures. *Phys. Rev. X* **2017**, *7* (2), 021026.

(65) Qiu, D. Y.; da Jornada, F. H.; Louie, S. G. Optical spectrum of MoS₂: many-body effects and diversity of exciton states. *Phys Rev Lett* **2013**, *111* (21), 216805.

(66) Gogoi, P. K.; Hu, Z.; Wang, Q.; Carvalho, A.; Schmidt, D.; Yin, X.; Chang, Y.-H.; Li, L.-J.; Sow, C. H.; Neto, A. H. C.; et al. Oxygen Passivation Mediated Tunability of Trion and Excitons in MoS₂. *Phys. Rev. Lett.* **2017**, *119* (7), 077402.

(67) Rusydi, A.; Rauer, R.; Neuber, G.; Bastjan, M.; Mahns, I.; Müller, S.; Saichu, P.; Schulz, B.; Singer, S. G.; Lichtenstein, A. I.; et al. Metal-insulator transition in manganites: Changes in optical conductivity up to 22 eV. *Physical Review B* **2008**, *78* (12), 125110.

(68) Birgeneau, R. J.; Chen, C. Y.; Gabbe, D. R.; Jenssen, H. P.; Kastner, M. A.; Peters, C. J.; Picone, P. J.; Thio, T.; Thurston, T. R.; Tuller, H. L.; et al. Soft-phonon behavior and transport in single-crystal La_2CuO_4 . *Phys. Rev. Lett.* **1987**, *59* (12), 1329-1332.

(69) Wilson, N. P.; Yao, W.; Shan, J.; Xu, X. Excitons and emergent quantum phenomena in stacked 2D semiconductors. *Nature* **2021**, *599* (7885), 383-392.

(70) Rivera, P.; Schaibley, J. R.; Jones, A. M.; Ross, J. S.; Wu, S.; Aivazian, G.; Klement, P.; Seyler, K.; Clark, G.; Ghimire, N. J.; et al. Observation of long-lived interlayer excitons in monolayer MoSe_2 - WSe_2 heterostructures. *Nat. Commun.* **2015**, *6* (1), 6242.

(71) Jiang, Y.; Chen, S.; Zheng, W.; Zheng, B.; Pan, A. Interlayer exciton formation, relaxation, and transport in TMD van der Waals heterostructures. *Light Sci. Appl.* **2021**, *10* (1), 72.

(72) Cooper, R. A.; Wang, Y.; Vignolle, B.; Lipscombe, O. J.; Hayden, S. M.; Tanabe, Y.; Adachi, T.; Koike, Y.; Nohara, M.; Takagi, H.; et al. Anomalous Criticality in the Electrical Resistivity of $\text{La}_{2-x}\text{Sr}_x\text{CuO}_4$. *Science* **2009**, *323* (5914), 603-607.

(73) Tang, C. S.; Zeng, S.; Wu, J.; Chen, S.; Naradipa, M. A.; Song, D.; Milošević, M. V.; Yang, P.; Diao, C.; Zhou, J.; et al. Detection of two-dimensional small polarons at oxide interfaces by optical spectroscopy. *Appl. Phys. Rev.* **2023**, *10* (3).

(74) Triana, C. A.; Granqvist, C. G.; Niklasson, G. A. Electrochromism and small-polaron hopping in oxygen deficient and lithium intercalated amorphous tungsten oxide films. *J. Appl. Phys.* **2015**, *118* (2).

(75) Emin, D. Optical properties of large and small polarons and bipolarons. *Physical Review B* **1993**, *48* (18), 13691-13702.

(76) Fratini, S.; Ciuchi, S. Dynamical Mean-Field Theory of Transport of Small Polarons. *Phys. Rev. Lett.* **2003**, *91* (25), 256403.

(77) Chen, X.; Lu, X.; Dubey, S.; Yao, Q.; Liu, S.; Wang, X.; Xiong, Q.; Zhang, L.; Srivastava, A. Entanglement of single-photons and chiral phonons in atomically thin WSe_2 . *Nat. Phys.* **2019**, *15* (3), 221-227.

(78) Chen, Z.; Wang, Y.; Rebec, S. N.; Jia, T.; Hashimoto, M.; Lu, D.; Moritz, B.; Moore, R. G.; Devereaux, T. P.; Shen, Z.-X. Anomalously strong near-neighbor attraction in doped 1D cuprate chains. *2021*, *373* (6560), 1235-1239.

(79) Li, J.; Jost, D.; Tang, T.; Wang, R.; Zhong, Y.; Chen, Z.; Garcia-Fernandez, M.; Pelliciari, J.; Bisogni, V.; Moritz, B.; et al. Doping Dependence of 2-Spinon Excitations in the Doped 1D Cuprate $\text{Ba}_2\text{CuO}_{3+\delta}$. *Phys. Rev. Lett.* **2025**, *134* (14), 146501.

(80) Jiang, M. Enhancing d-wave superconductivity with nearest-neighbor attraction in the extended Hubbard model. *Physical Review B* **2022**, *105* (2), 024510.

(81) Peng, C.; Wang, Y.; Wen, J.; Lee, Y. S.; Devereaux, T. P.; Jiang, H.-C. Enhanced superconductivity by near-neighbor attraction in the doped extended Hubbard model. *Physical Review B* **2023**, *107* (20), L201102.

(82) Zhang, L.; Guo, T.; Mou, Y.; Chen, Q.; Ma, T. Enhancement of d-wave pairing in the striped phase with nearest neighbor attraction. *Physical Review B* **2022**, *105* (15), 155154.

(83) Padma, H.; Thomas, J.; TenHuisen, S. F. R.; He, W.; Guan, Z.; Li, J.; Lee, B.; Wang, Y.; Lee, S. H.; Mao, Z.; et al. Beyond-Hubbard Pairing in a Cuprate Ladder. *Phys. Rev. X* **2025**, *15* (2), 021049.

(84) Wang, Y.; Chen, Z.; Shi, T.; Moritz, B.; Shen, Z.-X.; Devereaux, T. P. Phonon-Mediated Long-Range

Attractive Interaction in One-Dimensional Cuprates. *Phys. Rev. Lett.* **2021**, *127* (19), 197003.

(85) Meyer, T. L.; Jiang, L.; Park, S.; Egami, T.; Lee, H. N. Strain-relaxation and critical thickness of epitaxial $\text{La}_{1.85}\text{Sr}_{0.15}\text{CuO}_4$ films. *APL Materials* **2015**, *3* (12).

(86) Schranghamer, T. F.; Sharma, M.; Singh, R.; Das, S. J. C. S. R. Review and comparison of layer transfer methods for two-dimensional materials for emerging applications. *Chem. Soc. Rev.* **2021**, *50* (19), 11032-11054.

Figures and Tables

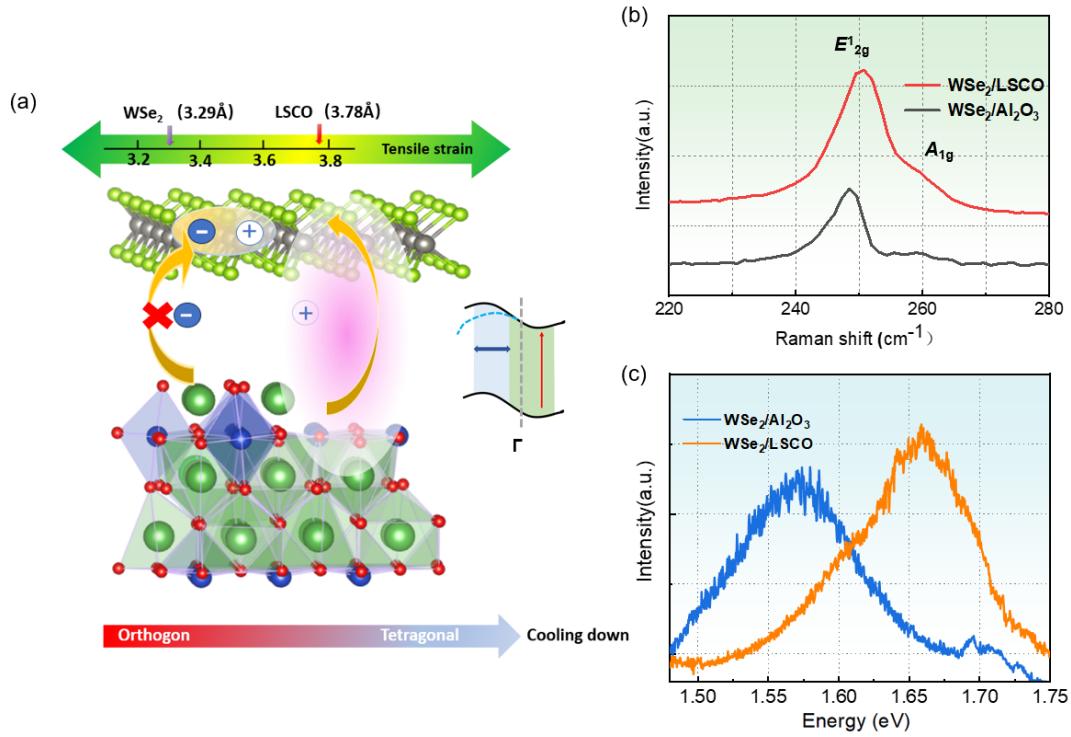


Figure 1. (a) Crystal model diagrams of monolayer-WSe₂/Al₂O₃ on 87.0 nm LSCO heterostructure. WSe₂ is subjected to tensile strain by the LSCO and a charge transfer occurs with the CuO₂ plane, resulting in the formation of interfacial polaron at the interface. This interfacial effect leads to the reduction in the band nesting structure (near the Γ point) of monolayer-WSe₂. Black curves in the band dispersion indicate a region where band nesting takes place. The red arrow indicate the direction of the optical transitions, which appear as peak C in the measured optical spectra. The blue arrow indicates the likely band region which is modified, thereby reducing the band nesting structure. (b) The Raman, and (c) photoluminescence spectra of monolayer-WSe₂/Al₂O₃ and WSe₂/LSCO.

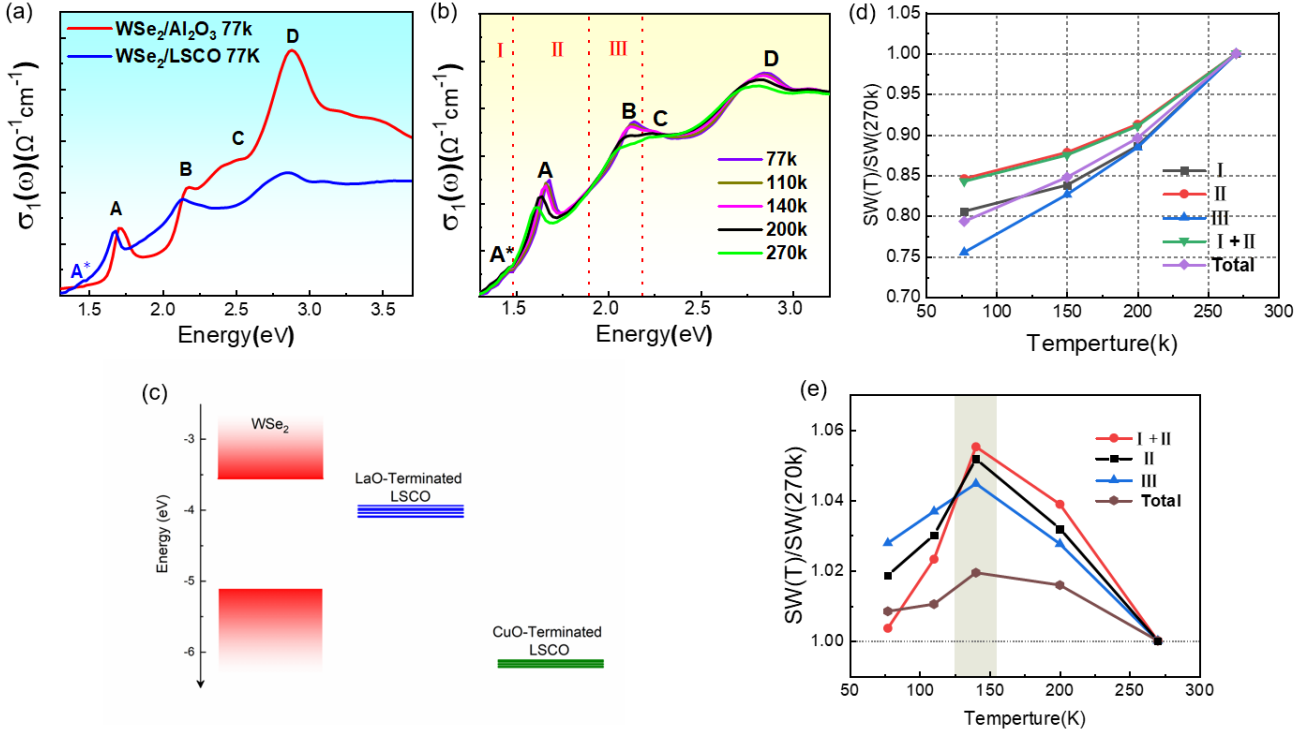


Figure 2. (a) Optical conductivity, $\sigma_1(\omega)$ of monolayer-WSe₂ and WSe₂/LSCO at 77K. (b) $\sigma_1(\omega)$ from 1.3 to 3.2 eV as a function of temperature for WSe₂/LSCO. (c) The alignment of the band edges of monolayer WSe₂ with the Fermi level of the LaO- and CuO-terminated LSCO surfaces based on Anderson's rule. (d) and (e) Spectral weights of monolayer-WSe₂/Al₂O₃ and monolayer-WSe₂/LSCO, respectively.

Integrated spectral weight $\frac{SW(T)}{SW(77K)}$ defined as $\frac{\int_{E_1}^{E_2} \sigma_1(E,T) dE}{\int_{E_1}^{E_2} \sigma_1(E,T=77\text{ K}) dE}$ in different spectral regions, I (1.30 – 1.48 eV), II (1.48 – 1.89 eV), and III (1.89 – 2.18 eV).

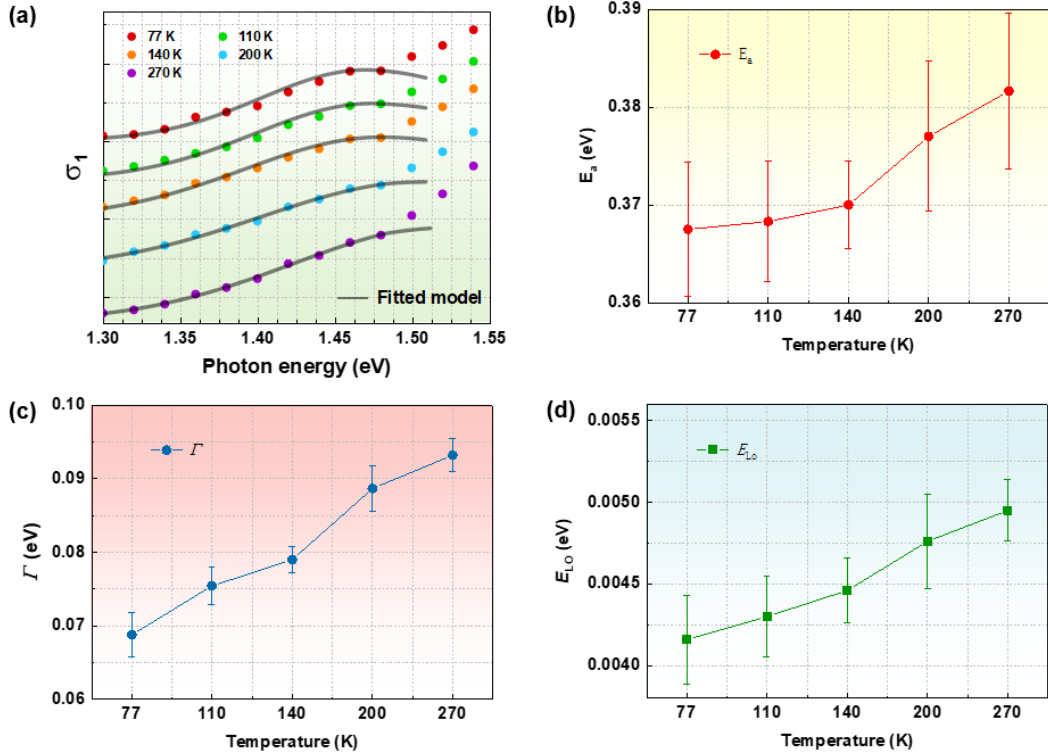


Figure 3. The zoom-in optical conductivity spectra σ_1 of WSe₂/LSCO heterostructure where optical feature A^* is present at different temperatures. (a) Overlay of the optical data and the fitted curve (dashed lines) based on the Bryksin small-polaron model (see supplementary Information). Parameters derived from Bryksin's small-polaron fitting analysis of the WSe₂/LSCO heterostructure. (b) Polaron hopping energy, E_a , (c) polaron bandwidth, Γ , and (d) phonon energy, E_{LO} .

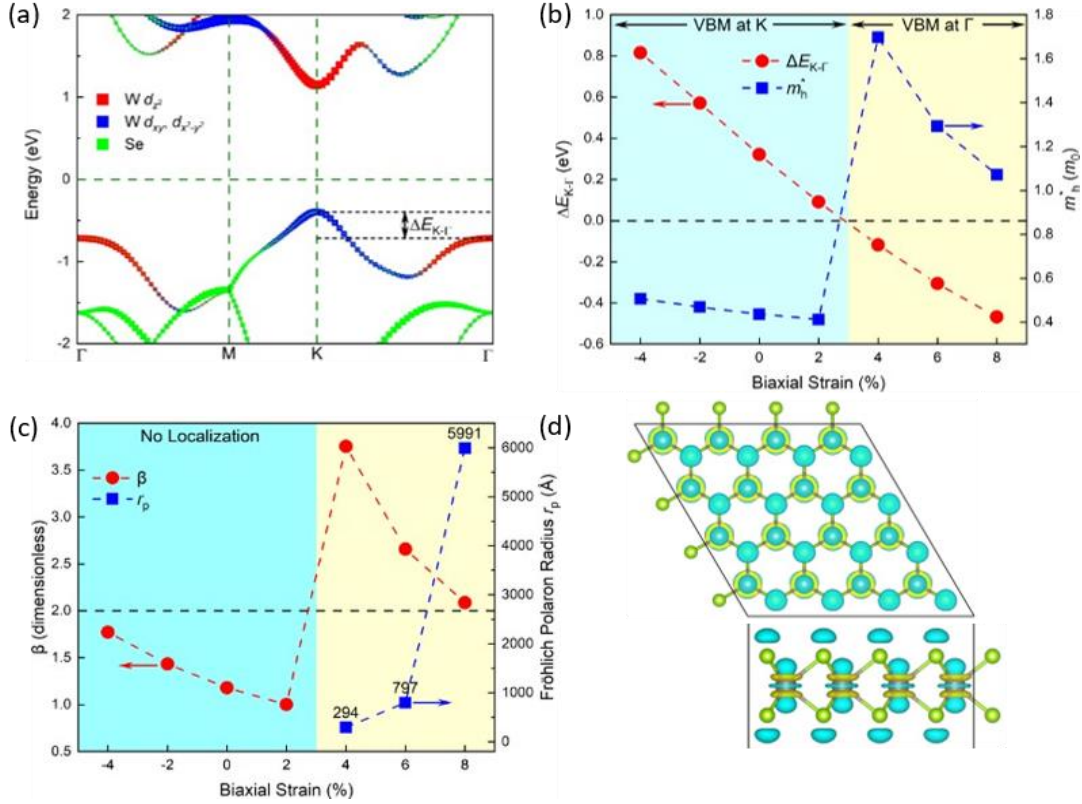


Figure 4. (a) The projected band structure of the strain-free WSe₂ at the PBE level of theory. (b) The energy difference between the highest valence state at the K - and Γ -points ($\Delta E_{K-\Gamma}$) and the hole effective mass around the valence band maximum as functions of the applied biaxial strain. (c) The polaron formation descriptor $\beta = \epsilon_{ion} m_h^* / m_0 a_0$ and the Fröhlich polaron radius as functions of the biaxial strain. Polarons do not form when $\beta \leq 2$. (d) The charge density difference between one hole-doped and charge-neutral states of the optimized 4 % strained $4 \times 4 \times 1$ WSe₂ supercell of which a W atom was selected and displaced from its equilibrium position before structural relaxation. Yellow and cyan iso-surfaces denote charge accumulation and depletion. The iso-value was set to $0.0005 \text{ e}/\text{\AA}^3$.